OPEN ACCESS
CellPress

Cell Reports
Report

Transmembrane Domain Targeting Peptide Antagonizing ErbB2/Neu Inhibits Breast Tumor Growth and Metastasis

Alexia Arpel,[1,5] Paul Sawma,[2] Caroline Spenlé,[1] Justine Fritz,[1] Lionel Meyer,[1] Norbert Garnier,[3] Inés Velázquez-Quesada,[1] Thomas Hussenet,[1] Samia Aci-Sèche,[3,4] Nadège Baumlin,[1] Monique Genest,[3] David Brasse,[5] Pierre Hubert,[2] Gérard Crémel,[1] Gertraud Orend,[1] Patrice Laquerrière,[5] and Dominique Bagnard[1,*]

[1]INSERM U 1109, Labex Medalis, Fédération de Médecine Translationnelle de Strasbourg (FMTS), Strasbourg University, Strasbourg 67200, France
[2]CNRS LISM UMR 7255, Aix Marseille University, Marseille 13402, France
[3]CNRS UPR 4301, Centre de Biophysique Moléculaire (CBM), Orleans University, Orleans F-45071, France
[4]ICOA UMR 7311, Orleans University, Orleans 45100, France
[5]CNRS UMR 7178, Institut Pluridisciplinaire Hubert Curien, Strasbourg University, Strasbourg 67037, France
*Correspondence: bagnard@unistra.fr
http://dx.doi.org/10.1016/j.celrep.2014.07.044

SUMMARY

Breast cancer is still a deadly disease despite major achievements in targeted therapies designed to block ligands or ligand-binding subunits of major tyrosine kinase receptors. Relapse is significant and metastases deleterious, which demands novel strategies for fighting this disease. Here, we report a proof-of-concept experiment demonstrating that small peptides interfering with the transmembrane domain of the tyrosine kinase epidermal growth factor receptor ErbB2 exhibit anticancer properties when used at micromolar dosages in a genetically engineered mouse model of breast cancer. Different assays demonstrate the specificity of the ErbB2-targeting peptide, which induces long-term reduction of ErbB2 phosphorylation and Akt signaling consistent with reduced tumor cell proliferation and increased survival. Microcomputed tomography analysis established the antimetastatic activity of the peptide and its impact on primary tumor growth. This reveals the interior of the cell membrane as an unexplored dimension for drug design.

INTRODUCTION

Breast tumorigenesis is a multistep process leading cells to undergo genetic and epigenetic transformations eventually giving rise to invasive carcinoma with bad prognosis (Bombonati and Sgroi, 2011). The ErbB family of tyrosine kinase receptors plays a key role in breast carcinogenesis through complex signaling networks made of multiple heterodimeric combinations of ErbB receptors (Eccles, 2011). Although having no identified ligand, ErbB2 is amplified and overexpressed in high-grade ductal carcinoma (Ross and Fletcher, 1999) and in high-grade inflammatory breast cancer (Charafe-Jauffret et al., 2004) thereby being largely involved in the induction and development of the malignant transformation (Freudenberg et al., 2009). Several studies revealed the importance of the dimeric status of ErbB2 triggering signaling cascades including the MAPK and PI3K/Akt pathways (Freudenberg et al., 2009). ErbB2 promotes cell proliferation, supports survival, and also favors invasion and metastasis. Most of the ErbB2-positive cancers resist to ErbB2-targeted therapies or tyrosine kinase inhibitors (Arteaga et al., 2012). The heterodimerization capacity of ErbB2 with ErbB1 or ErbB3 and activation of compensatory signaling pathways are considered as important resistance mechanisms (Yamaguchi et al., 2014). An ideal therapeutic strategy would hence be to interfere with receptor interactions by preventing dimerization and oligomerization in order to block redundant or compensatory downstream signaling pathways. Mounting evidence nowadays demonstrate that the transmembrane domains act as crucial regulators of integral membrane receptors interactions. Strikingly, the transmembrane domains of ErbB family members are also critically involved in ErbB signaling not only by stabilizing dimerization but also by controlling structural rearrangements favoring optimal conformational positioning for kinase activation (Cymer and Schneider, 2010). Hence, point mutations in the transmembrane domain of the murine homolog of ErbB2 (mErbB2 also called Neu) lead to constitutive activation of the receptor. This observation led Gullick and collaborators to show that expression in cells of short transmembrane mErbB2 proteins lacking any other interacting domains reduced cell growth both in vitro and in vivo (Lofts et al., 1993). Thus, blocking transmembrane-domain-dependent mErbB2 dimerization may represent an avenue for the design of a novel type of drugs with anticancer properties. Indeed, after successful inhibition of brain tumor growth when disrupting the nontyrosine kinase receptor Neuropilin-1 oligomerization by administration of a synthetic peptide antagonizing its transmembrane domain (Nasarre et al., 2010), we decided to explore how a similar strategy would apply for the inhibition of mErbB2 and how this may efficiently

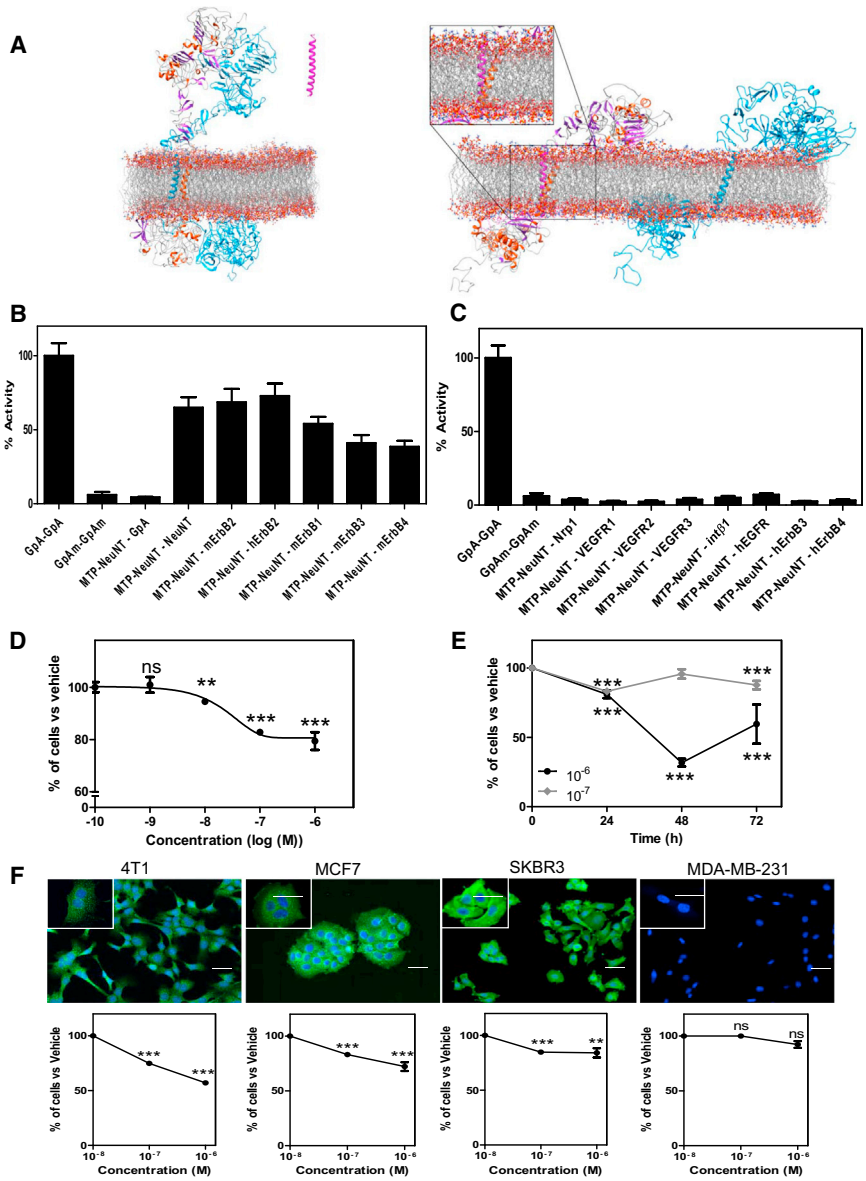

Figure 1. Demonstration of the Peptide-Based Inhibition of NeuNT/ErbB2 Receptor

(A) Analogy-based model of the nearly full-length monomeric and dimeric ErbB2 receptor illustrating the interaction between native transmembrane domains (TMDs) or with a peptide mimicking the TMD.

(B and C) Bacterial Adenylate Cyclase Two-Hybrid System demonstrating the specificity and capacity of positive (B) or negative (C) homo- or hetero-dimerization of NeuNT TMD.

(D) Demonstration of the dose-dependent anti-proliferative effect of MTP-NeuNT in NT193 cells derived from MMTV-NeuNT tumor-bearing mice using a MTT assay.

(E) Demonstration of the prolonged and intensified antiproliferative effect of the peptide over time.

(F) Proliferation assay (MTT) respectively from left to right on 4T1, MCF7, SKBR3, MDA-MB-231 cell lines treated with MTP-NeuNT or vehicle (LDS) at 10^{-7} and 10^{-6} M for 24 hr. Only cells expressing ErbB2 exhibit reduced proliferation when treated with the therapeutic peptide.

Data are presented as mean ± SEM from triplicate experiments. p values were determined by Mann-Whitney test in comparison to control LDS at 10^{-7} and 10^{-6} M for 24 hr. ***p < 0.0001, **p < 0.001 compared to vehicle. n.s., not significant. Scale bars, 50 μm. See also Table S1.

impact the metastatic process that remains nowadays the major challenge in breast cancer. We conducted this proof-of-concept experiment in an animal model of genetically induced breast tumors in which primary tumors are driven by the expression of a transforming mutant mErbB2 (NeuNT, exhibiting a mutation in its transmembrane domain leading to the constitutive activation of the receptor) oncogene under the MMTV mammary specific promoter (MMTV-NeuNT). Besides allowing the analysis in fully immune-competent mice, this model also gives rise to lung metastasis and has been clearly shown to be highly predictive of drug efficacy in human (Roberts et al., 2012). Here, we report that long-term triweekly intraperitoneal administration of low doses of a synthetic Membrane Targeting Peptide (MTP) mimicking the transmembrane domain of NeuNT (MTP-NeuNT) triggers sustained inhibition of the Akt pathway thereby impeding tumor cell growth and metastasis. Hence, this proof-of-concept experiment demonstrates that drugs targeting the transmembrane domain of tyrosine kinase receptors offer a credible alternative to classical approaches focused on extra or intracellular domains.

RESULTS AND DISCUSSION

Molecular Modeling of NeuNT Transmembrane Domain

The substitution of a valine for a glutamic acid in the transmembrane domain (TMD) of the mErbB2 receptor leads to the constitutive activation of the receptor in a dimeric state and carcinogenesis (Weiner et al., 1989). We first performed molecular modeling of TMD dimerizing interface to better predict the interaction of a TMD-NeuNT mimicking peptide (MTP-NeuNT) with the native TMD. Figure 1A shows the MTP-NeuNT in the context of the nearly full-length dimeric NeuNT receptor. This model is based on the recently published molecular dynamics study of EGFR dimers (Arkhipov et al., 2013). Our approach illustrates how the transmembrane domain kindly accommodates to the interface of the active receptor as previously suggested (Bagossi et al., 2005). Our model supports the idea of an active role of the TMD to control the proper dimeric and conformational organization of the receptor as recently described for EGFR (Endres et al., 2013). The crossing angle of the transmembrane helices at −45 degrees involves small residues in the core of the dimer. Such conformation was shown to be among the most stable in previously published ErbB2

TMD models (Bocharov et al., 2010). Thus, in the case of NeuNT receptor, MTP-NeuNT peptide would inhibit signaling by interfering with homodimerization of the TMD of the NeuNT receptor through direct competition for binding to the dimerization interface. When locked within the dimerization interface, MTP-NeuNT peptide would also prevent further heterodimerization by reducing its availability for any other interactions.

NeuNT Transmembrane Domain Sequence Exhibits Highly Specific Interactions

To address the specificity of MTP-NeuNT, we performed a two hybrid-like screening using the BACTH system (Karimova et al., 2001). Constructions encoding several TMD containing GxxxG motifs were used to measure interactions with NeuNT TMD (Figures 1B and 1C). This assay confirmed the high propensity of the MTP-NeuNT peptide to dimerize with NeuNT TMD when compared with positive control GPA-GPA (Glycophorin A) interaction or negative GPAm-GPAm interaction (mutated nondimerizing version of Glycophorin-A TMD in which glycine 83 is replaced by an isoleucine). NeuNT TMD sequence showed no heterodimerization with various GxxxG-containing sequences including Glycophorin A, Neuropilin-1, Vascular endothelial growth factor receptor 1, Vascular endothelial growth factor receptor 2, Vascular endothelial growth factor receptor 3, or Integrin Beta 1 (Figure 1C). The MTP-NeuNT sequence showed strong heterodimerization capacity with the mouse ErbB2 sequence (mErbB2) or the human ErbB2 sequences (hErbB2). Moreover, the NeuNT sequence significantly interacted with the murine orthologous of ErbB1 (mErbB1), ErbB3 (mErB3), and ErbB4 (mErbB4) but not with the human orthologous of these receptors (Figures 1B and 1C). Strikingly, using proximity ligation assay (Duolink system), we were able to show that MTP-NeuNT significantly reduced the number of ErbB2/ErbB3 dimer/oligomers in two different cell lines including the NeuNT and MCF7 cells (Figure S1). Thus, this part of the study confirmed stable homo- and heterodimer formation of the ErbB2 TMD (Bennasroune et al., 2004; Cymer and Schneider, 2010) and allowed us to define the dimerizing and antagonizing capability of the MTP-NeuNT peptide while demonstrating the specificity of interactions.

MTP-NeuNT Exhibits a Long-lasting Inhibitory Effect

There was no cellular model allowing the study of NeuNT signaling in a native context. To circumvent this issue, we developed a cell line derived from tumors collected in MMTV-NeuNT mice (NT193 cell line). This cell line exhibits epithelial and metastatic properties and constitutively expresses the mutated version of ErbB2. We performed a dose-response analysis to characterize the inhibition of cell proliferation that was obtained with 10^{-8} M of the peptide reaching a maximal effect at 10^{-6} M (−21% at 10^{-6} M versus vehicle, $p < 0.001$, Mann-Whitney test) (Figure 1D). Moreover, we found that treating the cells with 10^{-6} M had a prolonged and intensified effect as seen by a significant 2- to 3-fold amplification of the inhibitory effect when measuring cell proliferation at 48 and 72 hr post-treatment (−68% at 48 hr and −41% at 72 hr compared to control, $p < 0.001$ Mann-Whitney test). This long-lasting effect is dose dependent because 10^{-7} M of the MTP-NeuNT peptide only showed mild reduction over time (−17% at 24 hr, $p < 0.0001$ at 48 hr, $p = 0.24$, and −12% at 72 hr, $p < 0.0004$, compared to control, Mann-Whitney test) (Figure 1E). This persistent effect is consistent with our previous confocal microscopy observations demonstrating that similar TMD peptides enter the cells within a time frame of 30–50 min and that they can be imaged at the membrane up to 72 hr postincubation before endocytosis and degradation (Nasarre et al., 2010; Popot et al., 2011). Hence, we verified that MTP-NeuNT inhibited proliferation of another murine breast cancer cell line (4T1 cells) and ErbB2 expressing human breast cancer lines (MCF7, SKBR3) but had no effect on human MDA-MB-231 cells lacking expression of ErbB2 at the protein level (Figure 1F). Interestingly, partial knockdown of ErbB2 in MCF7 cells was correlated to decreased activity of MTP-NeuNT peptide (Figure 2A). The specificity of the peptide was also confirmed in gain-of-function experiments in which ErbB2 was expressed in MDA-MB-231 cells. Indeed, the proliferation of MDA-MB-231 ErbB2-positive cells was significantly decreased when treated with 10^{-6} M of MTP-NeuNT (Figure 2B).

MTP-NeuNT Inhibits ErbB2 Phosphorylation and Akt Phosphorylation

Because we observed an ErbB2-dependent negative impact of MTP-NeuNT on tumor cell expansion, we investigated how this peptide affects ErbB2 signaling. We observed a significant 45% reduction of ErbB2 phosphorylation (normalized to total ErbB2) in MTP-NeuNT-treated NT193 cells compared to control conditions (lithium dodecyl sulphate [LDS], $p = 0.0078$, Mann-Whitney test, Figure 2C) using a phosphospecific ELISA assay. Moreover, we also found a 58% decrease of Akt phosphorylation ($p < 0.0001$, chi-square test) in NT193 cells treated for 1 hr (Figure 2D). Strikingly, we found sustained inhibition of Akt phosphorylation up to 72 hr consistent with long-term inhibition of cell proliferation (Figure 2E). Similarly, Erk1/2 phosphorylation (the second most important signaling pathway triggered by NeuNT/ErbB2) was significantly reduced in the presence of the peptide (Figure 2E). Hence, MTP-NeuNT is able to inhibit the proproliferative and survival signaling cascades triggered by the NeuNT/ErbB2 receptor. From a therapeutic point of view, the inhibition of the Akt pathway highlights an interesting antitumoral potential of the peptide because the Akt pathway is hyperactive in more than 70% of breast cancers (Grunt and Mariani, 2013) and is considered as one of the major source of tumor cell survival and metastasis (Kim and Chung, 2002).

MTP-NeuNT Improves Overall Survival of MMTV-NeuNT Mice

MMTV-NeuNT transgenic mice develop stochastic mammary adenocarcinoma approximately from 12 weeks of age (Muller et al., 1988). To determine how MTP-NeuNT would affect breast tumor growth, we administrated intraperitoneal bolus of 15 μg/kg of the peptide (a concentration equivalent to 10^{-6} M) three times a week starting when the first palpable tumor reached a volume of 200 mm^3. Tumor occurrence was identical in both groups (100%) within a similar time frame to reach 200 mm^3 tumors (214 days in control versus 218 days in MTP-NeuNT group, $p = 0.95$, Mann-Whitney test) before administration of treatments. A waterfall plot of best response (determined between day 21

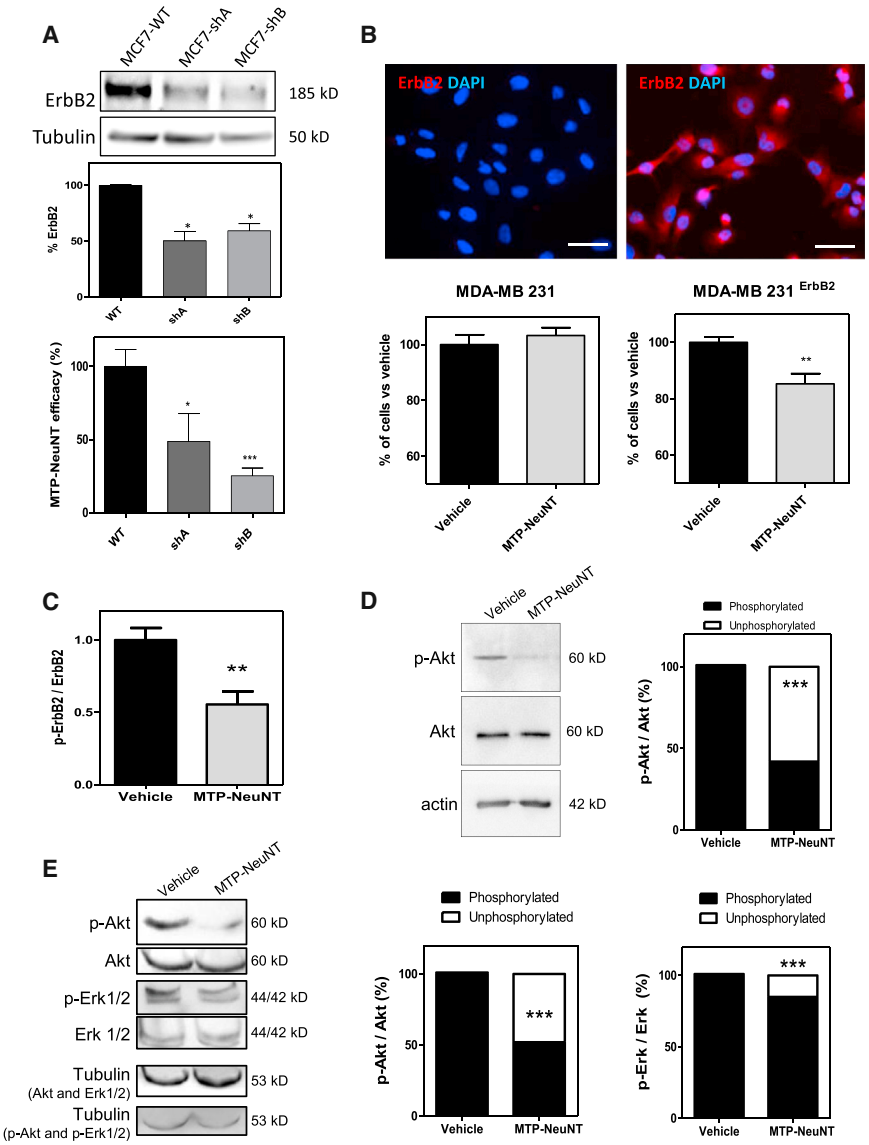

Figure 2. Characterization of MTP-NeuNT Inhibitory Effect

(A) We were able to generate two different clones of MCF7 cells partially knockdown for ErbB2. These clones showed reduced sensitivity to MTP-NeuNT almost proportional to the level of knockdown. Data are presented as mean ± SEM from triplicate experiments.

(B) To better confirm the link between cell sensitivity and expression level of ErbB2, we performed gain-of-function experiments in MDA-MB231 cells (lacking ErbB2 expression) becoming sensitive to MTP-NeuNT when expressing ErbB2. Data are presented as mean ± SEM from triplicate experiments.

(C) Demonstration of the inhibition of ErbB2 phosphorylation (ELISA assay). Data are presented as mean ± SEM from triplicate experiments.

(D) Akt phosphorylation (western blot) in NT193 cells treated with 10^{-6} M of MTP-NeuNT.

(E) Demonstration of the sustained inhibition of Akt phosphorylation after 2 days treatment also accompanied by significant reduction of Erk1/2 phosphorylation.

latency in MMTV-NeuNT mice (Yang et al., 2002). Thus, antagonizing the TMD of NeuNT appears as a potent therapeutic strategy.

Antimetastatic Activity of MTP-NeuNT

The occurrence of lung metastasis is a critical step in breast cancer progression and linked to disease-associated death (Chambers et al., 2002). Thus, we decided to monitor whether the improved survival of mice treated with MTP-NeuNT could reflect reduced lung metastatic colonization. To this end, we analyzed the serial μCT images collected at different time points of the protocol. Figure 3C is showing representative examples of the metastases detected in the control or the MTP-NeuNT-treated group. A waterfall plot of best response (determined between week 7 and week 8 of treatment according to the RECIST criteria) revealed that 100% of the treated animals responded to the treatment with 20% of SD and 80% with PR including two individuals above 90% of decrease in metastasis volume (Figure 3D). Quantitative measurements of the total number of metastasis in randomly selected five of ten control mice and five of ten MTP-NeuNT mice revealed a 2.4-fold decrease (n = 26 detectable metastases in control versus n = 11 metastases in MTP-NeuNT group) in treated animals after 8 weeks of treatment (Figure 3E). Determination of metastases volumes also revealed a 4.5-fold decrease when comparing cumulated volumes of metastases in mice of MTP-NeuNT group with those of the control group (cumulated volume CV = 78.3 mm^3 in control versus CV = 17.5 mm^3 in MTP-NeuNT group) (Figure 3F). Hence, and day 28 of treatment according to the RECIST criteria) revealed that 100% of the treated animals responded to the treatment with 33% of SD (stable disease, < −30% decrease of target lesion) and 67% with PR (partial response >30% decrease of target lesion) (Figure 3A). This high response rate translated into a marked survival benefit (Figure 3B) with a median survival increase up to 122% compared with untreated animals (73.5 days in control animals versus 90 days in MTP-NeuNT-treated animal, p = 0.0182, log-rank test). We also found that the delay for the appearance of second tumors (defined as the second palpated tumor) was doubled in MTP-NeuNT-treated mice as compared to control mice (4.6 days in control group versus 10.4 days in MTP-NeuNT-treated animals, p = 0.0066, Mann-Whitney test) thereby demonstrating an overall impact on disease progression. In comparison to our results for MTP-NeuNT that already reduced primary tumor onset and growth, a genetically delivered TGFβ antagonist had no effect on tumor

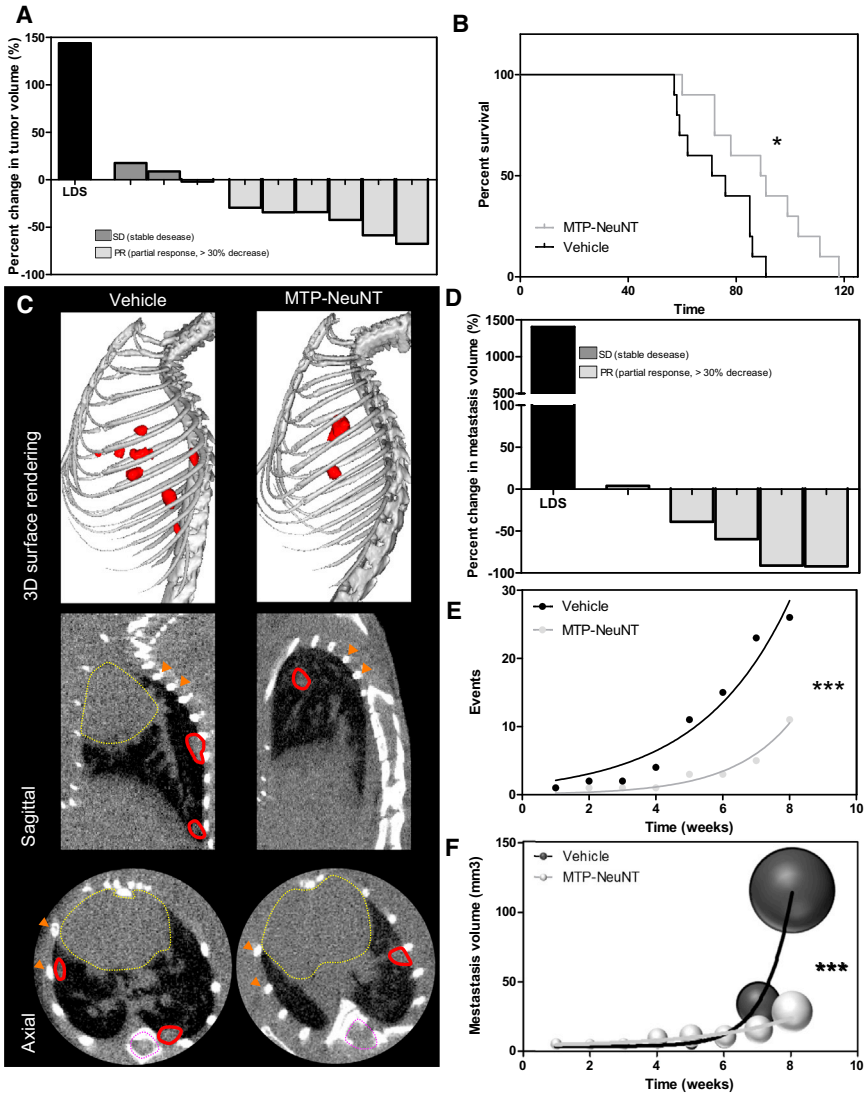

Figure 3. Effect of MTP-NeuNT In Vivo

(A) Demonstration of the inhibitory effect of NeuNT peptide on primary tumors volumes between day 21 and day 28 of treatment. The Waterfall graph represents the percent change in tumor volume of individual treated animals (gray bars, n = 9) compared to the averaged tumor volume increased determined in the control group (dark bar, n = 10). This demonstrates that 100% of the treated animals responded to the treatment with 30% stable disease and 70% partial response.

(B) Kaplan-Meyer survival curve demonstrating a significant increased survival of the treated animals compared to the control animals.

(C) Representative example of lung metastases seen from μCT 3D surface rendering or single sagittal and axial sections of the lungs in a control animal (left panel) and in a treated animal (right panel). Lung metastases are surrounded in red, heart in dashed yellow, and orange arrowheads point to ribs.

(D) Waterfall graph representing the percentage change in metastases volume of individual treated animals (gray bars, n = 5) compared to the averaged metastases volume increase determined in the control group (dark bar, n = 5) between weeks 7 and 8 of treatment.

(E and F) (E) Regression curves indicating that MTP-NeuNT treatment decreases the number of lung metastasis over time and (F) the cumulated volume of lung metastases.

μCT analysis revealed a significant antimetastatic effect of MTP-NeuNT characterized by both a reduction of the number and size of the lesions.

MTP-NeuNT Inhibits Metastasis Proliferation and Prevents Parenchymal Invasion

Because micrometastases (<1 mm in diameter) are difficult to analyze by μCT, we decided to perform histological examination of the lungs to further analyze the antimetastatic effect of MTP-NeuNT. This allowed us to confirm an overall 1.8-fold reduction of the mean number of lung metastasis (Figure 4A). Interestingly, a detailed analysis allowed us to distinguish between intravascular and parenchymal metastases (Siegel et al., 2003) to reveal a 2.6-fold decrease of the number of parenchymal metastases in the MTP-NeuNT-treated group compared to the control group. This result suggests that the peptide is able to reduce parenchymal invasion, presumably because impeding extravasation of metastasizing cells forming emboli in blood vessels. We also found a general 2.7-fold decrease of tumor cell proliferation in lung metastases using Ki67 staining (Figure 4B). Moreover, we observed a 1.9-fold increase of TUNEL-positive cells in the metastases of treated animals illustrating that the peptide impaired tumor cell survival (Figure 4C). Hence, Akt phosphorylation was 4.9-fold decreased (Figure 4D). Altogether these data demonstrate that the therapeutic peptide is able to slow down proliferation and extravasation of metastatic cells and survival as a consequence of Akt pathway inhibition.

Conclusions

We believe that the transmembrane domain of tyrosine kinase receptors is an eligible domain for drug design because this underestimated domain is crucial for the control of receptor activation (Arkhipov et al., 2013; Endres et al., 2013). Our study demonstrates that a peptide mimicking the TMD of the mutant mErbB2 (NeuNT) is able to specifically antagonize NeuNT, mouse and human ErbB2 thereby inhibiting phosphorylation of the receptor and downstream signaling. This long-lasting inhibitory property translated into improved survival and strong reduction of metastasis growth of mice presenting genetically induced mammary tumors. Strikingly, micromolar dosage was sufficient to trigger significant therapeutic benefit with no histological sign of toxicity (Figure S2). This unique strategy may apply to other tyrosine kinase receptors, therefore opening an avenue for drug design.

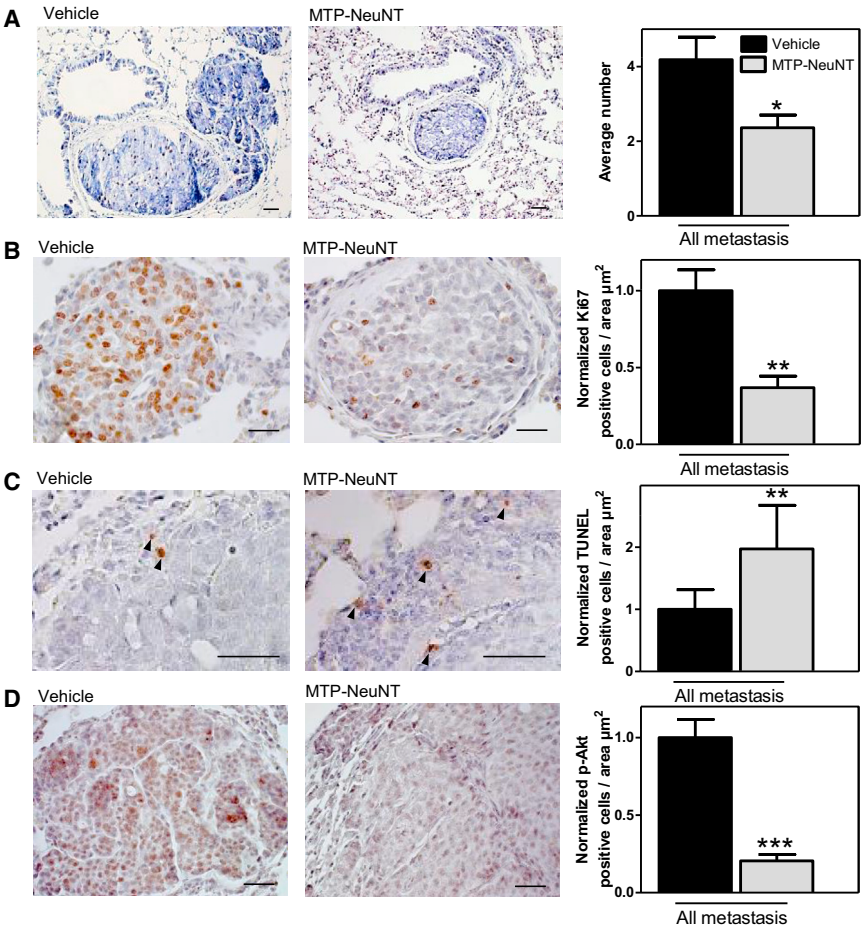

Figure 4. Histological Analysis of Lung Metastases

(A) Representative microphotographs illustrating extravasating metastasis and pure intravascular metastasis in the control and treated group, respectively. Systematic quantification of the number of metastasis reveals a 2-fold reduction in MTP-NeuNT-treated animals.

(B) Demonstration of the antiproliferative activity of the peptide by systematic counting of Ki67-positive cells.

(C) Demonstration of the proapoptotic effect of the peptide using the TUNEL method.

(D) Demonstration of the inhibition of the Akt pathway by systematic counting of phospho-Akt-positive cells in metastasis.

In (B)–(D), the left part is showing representative images of Ki67, TUNEL, or phospho-Akt-positive cells (immunocytochemistry, scale bars, 50 µm). The right parts are presenting the corresponding quantitation, p values are determined by Mann-Whitney test, *p < 0.05; **p < 0.001; ***p < 0.0001. Data are presented as mean ± SEM.

EXPERIMENTAL PROCEDURES

Cell Culture

All cell media were supplemented with 10% fetal calf serum (Gibco), 100 IU/ml penicillin, and 100 µg/ml streptomycin (Sigma), and cultures were performed at 37°C, 5% CO_2. MDA-MB-231 (ErbB2 negative), MCF7 (ErbB2 positive), SKBR3 (overexpressing ErbB2) cells were grown in Dulbecco's modified Eagle medium (DMEM, Gibco). Murine Balb/c 4T1 (ErbB2 positive) cells were grown in RPMI1640 (Gibco). NT193 cells were derived from MMTV-NeuNT primary tumors.

Peptides

Peptides have been synthesized by the Peptide Specialty Laboratories GmbH by automatic peptide synthesis (Fmoc chemistry). The peptide corresponding to the TM sequence of NeuNT: TFIIATVEGVLLFLILVVVVGILIKRR (in one-letter code, amino acid T^{654} to R^{680} according to Swissprot entry P06494) is referred as MTP-NeuNT. Peptides purity estimated by RP-HPLC was more than 90% according to manufacturer indication.

Modeling of the NeuNT Receptor Dimer and MTP-NeuNT

The nearly full length of the monomeric and the dimeric ErbB2 receptors were modeled by homology using MODELLER 9.11. The multitemplates strategy was employed using as templates the recent model of EGFR obtained by molecular dynamics and the X-rays and NMR structures of the domains available for the murine ErbB2 receptor. These domains are the extracellular region (PDB.ID 1N8Y), the kinase domain (PDB.ID 3PP0), and the right-handed dimer model of the TM domain. The 3D structure of the missing part of the intracellular domain of the murine ErbB2 was modeled using the prediction server I-TASSER. The homology models of the monomeric and the dimeric ErbB2 receptors were energetically minimized before their insertion in a lipidic bilayer.

Estimation of MTP-NeuNT Dimerization: BACTH Method

A bacterial two-hybrid system based on the recombination of adenylate cyclase CyaA from Bordetella pertussis was used to measure both homo- and heterodimerization propensities of transmembrane domains of interest. We have modified the BACTH pKTN25 and pUT18 plasmids so that they encode for hybrid proteins containing a signal sequence followed by the different TMDs of interest and the T25 and T18 fragments of adenylate cyclase. Double transformation in BTH101 (cya-) *E. coli* cells, cell growth and induction, and beta-Galactosidase assay in 96-well arrays were performed on a TECAN machine. Peptide sequences used in this study are summarized in Table S1.

Immunocytochemistry

Cells were grown on sterile glass coverslips for 1 day before immunofluorescence staining. The cells were fixed with 4% formaldehyde (FA) for 10 min. The samples were gently rinsed with PBS before adding the blocking solution (FCS 5%) for a minimum of 30 min. Cells were permeabilized using 1 × PBS with 0.1% Tween 20 for 5 min. Primary HER2/ErbB2 (Cell Signaling #2242, diluted 1/50 from stock solution) antibody diluted in 5% fetal calf serum (FBS)-PBS was added to the cell over night at room temperature (RT). After three washes of 5 min secondary antibody (donkey anti-rabbit, Jackson ImmunoResearch 711-165-152 diluted 1/1,000 from stock) was added at RT for 90 min. After washing in PBS, the cell nuclei were stained with DAPI (4′,6-diamidino-2-phenylindole, 1/30,000 in water) for 10 min. Glass coverslips were finally mounted on microscopy glass slides using a polymerization medium (FluorSave reagent, Calbiochem-Merck cat# 345789).

Histology

Giemsa Staining

Lungs (left lobes) were removed and fixed overnight in 4% FA. Following extensive washes organs were dehydrated in 100% ethanol for a day and then embedded in paraffin. Samples were stored at RT. The paraffin-embedded tissue blocks sections (7 µm thickness) were dewaxed and rehydrated through

100% Toluene (2 washes of 15 min) then 100%–70% alcohol (10 min each) and then stained with Giemsa stain (RAL#320310-0125, diluted 1/50 from stock solution) for 2 hr at 37°C. After extensive washing, differentiation is achieved with 0.5% aqueous acetic solution for 30 s. Sections are then rapidly dehydrated in 70%–100% alcohol baths with rapid dips in each bath before final wash in toluene for 15 min. Slides were mounted in Eukitt (Sigma) for long term conservation and microscopic observation.

Hematoxylin-Eosin

The paraffin embedded kidney and liver sections were dewaxed and rehydrated as described above. Sections were stained with hematoxylin (Surgipath #01562E) for 5 min and washed with running tap water. Differentiation was accomplished in acid alcohol solution for 7 s followed by thorough wash (running tap water for at least 10 min). Sections were incubated in eosin (Harris, RAL# 31273-7) for 10 s, rinsed again, and dehydrated as described above before mounting in Eukitt (Sigma #03989).

Cell Proliferation

In vitro cell proliferation was monitored using MTT (3-[4,5 -Dimethylthiazol-2 -yl]-2,5-di phenyl tetrazolium bromide) proliferation assay according to manufacturer's instruction (Sigma, M2128). Optical density was determined at 570 nm using an ELISA plate reader spectrophotometer (EL800, BioTek Instruments). NT193 cells were seeded at a density of 10,000 cells per well in a 96-well plate; the cells were then incubated with various peptide concentrations (ranging from 10^{-9} to 10^{-6} M) or corresponding vehicle (LDS, ranging from 0.72 to 720 μM). In vivo cell proliferation was determined by quantification of Ki67-positive cells. Dewaxed sections were boiled with the antigen retrieval sodium citrate buffer (pH 6) for 20 min (Sigma #CO759). After incubation with blocking solution (PBS Triton-100X +5% NGS) for 20 min, the avidin/biotin blocking solutions were added on the tissue for 15 min, respectively (Blocking kit from Vector Laboratories SP-2001). The primary anti-Ki67 antibody (Thermo Scientific, RM-9106) was added in blocking solution overnight at a dilution of 1/200, whereas secondary antibody (goat anti-rabbit, Vector Laboratories, #PI-1000) was added at a dilution of 1/200 in PBS for 1 hr at room temperature. Revelation was performed using Elit Vectastain kit (PK-6100). All specimens were counterstained with hematoxylin.

Determination of Apoptosis

Sections were prepared as above to determine apoptosis using the ApopTag Plus Peroxidase In situ Hybridization and Detection Kit (Chemicon, S7101) according to the manufacturer's instructions. The number of positive cells was counted on a total of eight sections of the control group and eight sections of the MTP-NeuNT-treated group. Data were expressed as the number of positive (apoptotic) cells per area (μm^2).

Image Acquisition

Cell fluorescence images were acquired with the fluorescence Zeiss Imager Z2 equipped with HXP 120 W lamp and ApoTome system. Lung metastasis images were acquired using a macroscope Zeiss AXIOZoom.V16. Images were analyzed using AxioVision 4.7.2 (Zeiss), Zen (Zeiss), and Image J (Wayne Rasband, NIH) software.

Phosphorylation of ErbB2 Receptor on NT193 Cells

Phospho-Neu (Y1221/Y1222) cell-based colorimetric ELISA Kit (Immunoway Biotechnology Company) was used to monitor levels of phosphorylated mErbB2 and related total mErbB2 receptor. NT193 cells were seeded into the wells of the 96-well plate at densities of 30,000 cells in 200 μl cell-culture media and serum starved overnight. The cells were then treated with either vehicle (LDS 720 μM) or MTP-NeuNT peptide for 1 hr at 10^{-6} M. mErbB2 phosphorylation was assessed according to the manufacturer's instructions.

Western Blot

Before protein extraction, the cells were treated either with 10^{-6} M of MTP-NeuNT or Vehicle (LDS, 720 μM). Protein sample preparation was completed with Laemmli buffer supplemented with protease inhibitor (Roche tablets, #11836145001) and 5 mM of Na orthovanadate. Proteins were resolved in an 8% SDS/PAGE gel and transferred onto a nitrocellulose membrane (Whatman). The blots were soaked in blocking solution (TBS/1% Tween 20/5% milk) for 1 hr at RT. First antibodies (rabbit anti-phospho-akt, Rabbit anti-akt, Cell Signaling #4060 and #9272, respectively) and mouse antiactin (Chemicon #MAB1501R) were incubated overnight at 4°C. Secondary antibodies (anti-rabbit-HRP, GE Healthcare, #NA934V and anti-mouse-HRP, GE Healthcare, #NXA931) were incubated 1 hr a RT in TBS/1% Tween 20/5% milk. The revelation step was performed using streptavidin-biotinylated horseradish peroxidase complex (Amersham #RPN1051) according to the manufacturer instructions. Images of the immune blots were acquired and analyzed thanks to the GENE GNOME apparatus (Syngene Bio Imaging).

Loss- and Gain-of-Function Experiments

Lentiviruses producing HEK293T cells were transfected using the JetPEI transfection reagent (PolyPlus Transfection) with a set of two different pGFP-C-shLenti 29MER plasmid vectors: TL320342A, TL320342B (OriGene) and three lentivirus packaging plasmid vectors containing pMDL g/p RRE, pRSV-rev, pMD2-VSVG (Addgene). After 48 hr, the HEK293T cells culture media was harvested and transferred on MCF7 cells growth media containing 8 μg/ml protamine sulfate (Sigma-Aldrich) for 72 hr prior to selection with 5 μg/ml puromycin. Screening of protein knockdown was done by western blot as described above.

Gain-of-Function Experiment

MDA-MB-231 (negative for HER2 and not sensitive to MTP-NeuNT) were transfected with a plasmid vector PSV2neo carrying the sequence coding for the human version of HER2 receptor. The transfection of MDA-MB231 was done with the JetPEI (Polyplus Transfection) reagent according to the manufacturer procedure. Cells were then selected with geneticin sulfate G418 (Life Technologies) for 10 days before using them for functional assays.

Animal Handling and In Vivo Ethical Statement

Experiments were performed according to the Guide for Care and Use of Laboratory Animals (E67-6-482-21) and the European Directive with approval of the regional ethical committee (reference AL/55/62/02/13). Mice received food and water ad libitum. Animals were sacrificed using CO_2. All necessary precautions were taken to minimize pain or discomfort of the animals. General health status was monitored three times a week by independent observers. Sacrifice of the animal was effectuated when reaching limit ethical endpoints.

Production of the Transgenic MMTV-NeuNT Mice

Transgenic FVB mice expressing the mutant activated form of murine ErbB2 (NeuNT) under control of the mouse mammary tumor virus (MMTV) promoter (Muller et al., 1988) were kindly obtained from Dr. Gerhard Christofori (University of Basel). We generated a cohort of 20 mice receiving either 15 μg/kg of MTP-NeuNT or vehicle (LDS, 720 μM) three times a week. Treatments were administrated when the first palpated tumor reached 200 mm^3 volume as determined using electronic caliper.

In Vivo Imaging and Surface Rendering of μCT

In vivo μCT, equipped with dedicated anesthesia chamber, was performed on a weekly basis at the IPHC (Institut Pluridisciplinaire Hubert Curien), Strasbourg, France. Acquisition parameters were 40 kVp, 250 lA, and 235 ms exposures per projection in binning 2 × 2 with a projection pixel size of 100 × 100 cm^2. A full image data set covered 360° in 0.47° steps for a total of 768 projections. Images were reconstructed with a cone-beam reconstruction algorithm producing in real time a 3D image with an isotropic voxel size of 0.1 mm. The delivered dose during each microCT exam was 48 mGy. Once the metastasis was detected in the lung, its volume was calculated as follows: $V = (4/3) * \pi * rx * ry * rz$, where r is the radius of the metastasis and x, y, z are the axial directions.

Statistics

Statistical analyses were performed using Mann-Whitney test (for sample $n < 30$), chi-square analysis (for qualitative data), extra sum of square F test (for the μCT number of metastasis curves) using GraphPad software. p values are given in the figure legends, and values of $p < 0.05$ were considered to be statistically significant. A minimum of three independent experiments was

performed for in vitro assays (proliferation, ErbB2 phosphorylation, and western blot). For in vivo experiments, the sample size calculation anticipated a therapeutic effect of 20% for a SD of 14% and confidence interval of confidence 95% (Lamorte's Power calculation, University of Boston).

SUPPLEMENTAL INFORMATION

Supplemental Information includes two figures and one table and can be found with this article online at http://dx.doi.org/10.1016/j.celrep.2014.07.044.

AUTHOR CONTRIBUTIONS

A.A. performed animal studies, in vitro assays, histology and staining, western blots, and data analysis; P.S. and P.H. conducted BACTH assays and related analysis; C.P. performed western blots and Duolink assays; J.F. and L.M. performed loss- and gain-of-function experiments, N.G., S.A.-S., and M.G. performed modeling of Neu receptor; I.V.-Q., T.H., and G.O. produced and validated the NeuNT cell line, G.C. was in charge of peptide production, control, and solubilization; D. Brasse and P.L. supervised and designed μCT imaging and analysis; D. Bagnard designed the study, coordinated the project, and analyzed data.

ACKNOWLEDGMENTS

The authors are grateful to D. Gerhard Christofori for providing the MMTV-NeuNT model and to Florian Busso and Abdoul Ahad Ould Sidi for excellent technical support for the 3D surface rendering of lung metastastases. This work was supported by INCA to G.O., ANR -10-BLAN-1507 to D. Bagnard/P.H./M.G., and Ligue Régionale contre le Cancer to D. Bagnard. This work has been published within the LABEX ANR-10-LABX-0034_Medalis and received a financial support from French government managed by "Agence National de la Recherche" under "Programme d'investissement d'avenir."

Received: July 17, 2013
Revised: May 27, 2014
Accepted: July 24, 2014
Published: September 11, 2014

REFERENCES

Arkhipov, A., Shan, Y., Das, R., Endres, N.F., Eastwood, M.P., Wemmer, D.E., Kuriyan, J., and Shaw, D.E. (2013). Architecture and membrane interactions of the EGF receptor. Cell *152*, 557–569.

Arteaga, C.L., Sliwkowski, M.X., Osborne, C.K., Perez, E.A., Puglisi, F., and Gianni, L. (2012). Treatment of HER2-positive breast cancer: current status and future perspectives. Nat Rev Clin Oncol *9*, 16–32.

Bagossi, P., Horváth, G., Vereb, G., Szöllösi, J., and Tözsér, J. (2005). Molecular modeling of nearly full-length ErbB2 receptor. Biophys. J. *88*, 1354–1363.

Bennasroune, A., Fickova, M., Gardin, A., Dirrig-Grosch, S., Aunis, D., Crémel, G., and Hubert, P. (2004). Transmembrane peptides as inhibitors of ErbB receptor signaling. Mol. Biol. Cell *15*, 3464–3474.

Bocharov, E.V., Volynsky, P.E., Pavlov, K.V., Efremov, R.G., and Arseniev, A.S. (2010). Structure elucidation of dimeric transmembrane domains of bitopic proteins. Cell Adhes. Migr. *4*, 284–298.

Bombonati, A., and Sgroi, D.C. (2011). The molecular pathology of breast cancer progression. J. Pathol. *223*, 307–317.

Chambers, A.F., Groom, A.C., and MacDonald, I.C. (2002). Dissemination and growth of cancer cells in metastatic sites. Nat. Rev. Cancer *2*, 563–572.

Charafe-Jauffret, E., Tarpin, C., Bardou, V.-J., Bertucci, F., Ginestier, C., Braud, A.-C., Puig, B., Geneix, J., Hassoun, J., Birnbaum, D., et al. (2004). Immunophenotypic analysis of inflammatory breast cancers: identification of an 'inflammatory signature'. J. Pathol. *202*, 265–273.

Cymer, F., and Schneider, D. (2010). Transmembrane helix-helix interactions involved in ErbB receptor signaling. Cell Adhes. Migr. *4*, 299–312.

Eccles, S.A. (2011). The epidermal growth factor receptor/Erb-B/HER family in normal and malignant breast biology. Int. J. Dev. Biol. *55*, 685–696.

Endres, N.F., Das, R., Smith, A.W., Arkhipov, A., Kovacs, E., Huang, Y., Pelton, J.G., Shan, Y., Shaw, D.E., Wemmer, D.E., et al. (2013). Conformational coupling across the plasma membrane in activation of the EGF receptor. Cell *152*, 543–556.

Freudenberg, J.A., Wang, Q., Katsumata, M., Drebin, J., Nagatomo, I., and Greene, M.I. (2009). The role of HER2 in early breast cancer metastasis and the origins of resistance to HER2-targeted therapies. Exp. Mol. Pathol. *87*, 1–11.

Grunt, T.W., and Mariani, G.L. (2013). Novel approaches for molecular targeted therapy of breast cancer: interfering with PI3K/AKT/mTOR signaling. Curr. Cancer Drug Targets *13*, 188–204.

Karimova, G., Ullmann, A., and Ladant, D. (2001). Protein-protein interaction between Bacillus stearothermophilus tyrosyl-tRNA synthetase subdomains revealed by a bacterial two-hybrid system. J. Mol. Microbiol. Biotechnol. *3*, 73–82.

Kim, D., and Chung, J. (2002). Akt: versatile mediator of cell survival and beyond. J. Biochem. Mol. Biol. *35*, 106–115.

Lofts, F.J., Hurst, H.C., Sternberg, M.J., and Gullick, W.J. (1993). Specific short transmembrane sequences can inhibit transformation by the mutant neu growth factor receptor in vitro and in vivo. Oncogene *8*, 2813–2820.

Muller, W.J., Sinn, E., Pattengale, P.K., Wallace, R., and Leder, P. (1988). Single-step induction of mammary adenocarcinoma in transgenic mice bearing the activated c-neu oncogene. Cell *54*, 105–115.

Nasarre, C., Roth, M., Jacob, L., Roth, L., Koncina, E., Thien, A., Labourdette, G., Poulet, P., Hubert, P., Crémel, G., et al. (2010). Peptide-based interference of the transmembrane domain of neuropilin-1 inhibits glioma growth in vivo. Oncogene *29*, 2381–2392.

Popot, J.-L., Althoff, T., Bagnard, D., Banères, J.-L., Bazzacco, P., Billon-Denis, E., Catoire, L.J., Champeil, P., Charvolin, D., Cocco, M.J., et al. (2011). Amphipols from A to Z. Annu Rev Biophys *40*, 379–408.

Roberts, P.J., Usary, J.E., Darr, D.B., Dillon, P.M., Pfefferle, A.D., Whittle, M.C., Duncan, J.S., Johnson, S.M., Combest, A.J., Jin, J., et al. (2012). Combined PI3K/mTOR and MEK inhibition provides broad antitumor activity in faithful murine cancer models. Clin. Cancer Res. *18*, 5290–5303.

Ross, J.S., and Fletcher, J.A. (1999). The HER-2/neu oncogene: prognostic factor, predictive factor and target for therapy. Semin. Cancer Biol. *9*, 125–138.

Siegel, P.M., Shu, W., Cardiff, R.D., Muller, W.J., and Massagué, J. (2003). Transforming growth factor beta signaling impairs Neu-induced mammary tumorigenesis while promoting pulmonary metastasis. Proc. Natl. Acad. Sci. USA *100*, 8430–8435.

Weiner, D.B., Kokai, Y., Wada, T., Cohen, J.A., Williams, W.V., and Greene, M.I. (1989). Linkage of tyrosine kinase activity with transforming ability of the p185neu oncoprotein. Oncogene *4*, 1175–1183.

Yamaguchi, H., Chang, S.-S., Hsu, J.L., and Hung, M.-C. (2014). Signaling cross-talk in the resistance to HER family receptor targeted therapy. Oncogene *33*, 1073–1081.

Yang, Y.-A., Dukhanina, O., Tang, B., Mamura, M., Letterio, J.J., MacGregor, J., Patel, S.C., Khozin, S., Liu, Z.-Y., Green, J., et al. (2002). Lifetime exposure to a soluble TGF-beta antagonist protects mice against metastasis without adverse side effects. J. Clin. Invest. *109*, 1607–1615.